





Gravitational Wave in $f(R)$ Gravity: Possible Signature of Sub- and Super-Chandrasekhar Limiting-mass White Dwarfs

Surajit Kalita  and Banibrata Mukhopadhyay 

Department of Physics, Indian Institute of Science, Bangalore 560012, India; surajitk@iisc.ac.in, bm@iisc.ac.in

Received 2020 November 16; revised 2021 January 5; accepted 2021 January 18; published 2021 March 8

Abstract

After the prediction of many sub- and super-Chandrasekhar (at least a dozen for the latter) limiting-mass white dwarfs (WDs), hence apparently a peculiar class of WDs, from the observations of luminosity of Type Ia supernovae, researchers have proposed various models to explain these two classes of WD separately. We earlier showed that these two peculiar classes of WD, along with the regular WD, can be explained by a single form of the $f(R)$ gravity, whose effect is significant only in the high-density regime, and it almost vanishes in the low-density regime. However, since there is no direct detection of such a WD, it is difficult to single out one specific theory from the zoo of modified theories of gravity. We discuss the possibility of direct detection of such a WD in gravitational wave (GW) astronomy. It is well known that in $f(R)$ gravity more than two polarization modes are present. We estimate the amplitudes of all the relevant modes for the peculiar and the regular WD. We further discuss the possibility of their detections through future-based GW detectors, such as LISA, ALIA, DECIGO, BBO, or the Einstein Telescope, and thereby put constraints on or rule out various modified theories of gravity. This exploration links the theory with possible observations through GW in $f(R)$ gravity.

Unified Astronomy Thesaurus concepts: [White dwarf stars \(1799\)](#); [Gravitational waves \(678\)](#); [Scalar-tensor-vector gravity \(1428\)](#); [Chandrasekhar limit \(221\)](#); [Rotation powered pulsars \(1408\)](#); [Stellar magnetic fields \(1610\)](#); [Stellar surfaces \(1632\)](#)

1. Introduction

White dwarfs (WDs) are the end state of stars with mass $\lesssim 8M_{\odot}$. A WD attains its stable equilibrium configuration by balancing the outward force due to the degenerate electron gas with the inward force of gravity. If the WD has a binary companion, it pulls out matter from the companion, and as a result, the mass of WD increases. Once the mass of the WD reaches the Chandrasekhar mass limit (Chandrasekhar 1931; $\sim 1.4M_{\odot}$ for carbon-oxygen nonrotating, nonmagnetized WDs), the pressure balance no longer sustains, and the WD bursts out to produce a Type Ia supernova (SN Ia; Choudhuri 2010). The similarity in peak luminosities of SNe Ia is used as one of the standard candles to estimate the luminosity distances for various astronomical and cosmological objects (Lieb & Yau 1987; Nomoto et al. 1997). However, recent discoveries of various under- and overluminous SNe Ia question the complete validity of considering luminosities of SNe Ia as standard candles. SNe Ia such as SN 1991bg (Filippenko et al. 1992; Mazzali et al. 1997), SN 1997cn (Turatto et al. 1998), SN 1998de (Modjaz et al. 2001), SN 1999by (Garnavich et al. 2004), and SN 2005bl (Taubenberger et al. 2008) were discovered with extremely low luminosities, which were produced from WDs with ^{56}Ni mass content as low as $\sim 0.1M_{\odot}$ (Stritzinger et al. 2006). On the other hand, a different class of SNe Ia, such as SN 2003fg (Howell et al. 2006), SN 2006gz (Hicken et al. 2007), SN 2009dc (Yamanaka et al. 2009; Tanaka et al. 2010; Silverman et al. 2011; Taubenberger et al. 2011; Kamiya et al. 2012), SN 2007if (Scalzo et al. 2010; Yuan et al. 2010; Scalzo et al. 2012), SN 2013cv (Cao et al. 2016), and many more were discovered with an excess luminosity, with the observed mass of ^{56}Ni as high as $\sim 1.8M_{\odot}$ (Kamiya et al. 2012), violating the Khokhlov pure detonation limit (Khokhlov et al. 1993). It was inferred that these underluminous SNe Ia were produced from WDs with a mass $\sim 0.6M_{\odot}$ (Mazzali et al. 1997; Turatto et al. 1998), while the same for overluminous SNe Ia could be $\sim 2.8M_{\odot}$ (Scalzo et al. 2010; Kamiya et al. 2012).

Hence, these progenitor WDs of peculiar SNe Ia violate the Chandrasekhar mass limit: the underluminous SNe Ia were produced from sub-Chandrasekhar limiting-mass WDs (WDs burst before reaching the mass $\sim 1.4M_{\odot}$), and the overluminous SNe Ia were produced from super-Chandrasekhar limiting-mass WDs (WDs burst well above the mass $\sim 1.4M_{\odot}$). These new mass limits are important, as they may lead to modifying the standard candle.

Various groups around the world have proposed different models to explain the formation of these two peculiar classes of SNe Ia. Sub-Chandrasekhar limiting-mass WDs were believed to be formed by merging two sub-Chandrasekhar mass WDs (double-degenerate scenario), leading to another sub-Chandrasekhar mass WD, exploding due to accretion of a helium layer (Hillebrandt & Niemeyer 2000; Pakmor et al. 2010). On the other hand, the super-Chandrasekhar WDs were often explained by incorporating different physics, such as a double-degenerate scenario (Hicken et al. 2007), presence of magnetic fields (Das & Mukhopadhyay 2013, 2014), presence of a differential rotation (Hachisu et al. 2012), presence of charge in the WDs (Liu et al. 2014), ungravity effect (Bertolami & Mariji 2016), lepton number violation in magnetized WD (Belyaev et al. 2015), generalized Heisenberg uncertainty principle (Ong 2018), and many more. However, none of these theories can self-consistently explain both of the peculiar classes of WDs. Moreover, each of these has some caveats or incompleteness, mostly based on the stability (Komatsu et al. 1989; Braithwaite 2009). Furthermore, numerical simulations showed that a merger of two massive WDs could never lead to a mass as high as $2.8M_{\odot}$ owing to the off-center ignition and formation of a neutron star rather than an (overluminous) SN Ia (Saio & Nomoto 2004; Martin et al. 2006). Hence, all the conventional pictures failed to explain the inferred masses of both the sub- and super-Chandrasekhar progenitor WDs and also both classes of progenitor WDs simultaneously by invoking the same

physics. Moreover, each of the theories can explain only one regime of SN Ia, but it seems more likely that the nature would prefer only one scenario/physics to exhibit the same class of SNe. Whether it be an under- or overluminous SN Ia, other physics such as the presence of Si, etc., remains the same. Therefore, we seem to require just one theory to explain all the SNe Ia.

Einstein's theory of general relativity (GR) is undoubtedly the most beautiful theory to explain the theory of gravity. It can easily explain a large number of phenomena where Newtonian gravity falls short, such as the deflection of light in strong gravity, generation of the gravitational wave (GW) in $3 + 1$ dimension, perihelion precession of Mercury's orbit, and gravitational redshift of light, to mention a few. It is well known that in the asymptotically flat limit where the typical velocity is much smaller than the speed of light, GR reduces to the Newtonian theory of gravity (Ryder 2009). According to the Newtonian theory, the Chandrasekhar mass limit for WDs is achieved only at zero radius with infinite density, whereas GR can consistently explain this for a WD with a finite radius and a finite density (Padmanabhan 2001). Nevertheless, following several recent observations in cosmology (Joyce et al. 2016; Casas et al. 2017) and in the high-density regions of the universe, such as at the vicinity of compact objects (Held et al. 2019; Banerjee et al. 2020a, 2020b; Moffat 2020), it seems that GR may not be the ultimate theory of gravity. Starobinsky (1980) first used one of the modified theories of gravity, namely, R^2 -gravity, with R being the scalar curvature, to explain the cosmology of the very early universe. Eventually, researchers have proposed a large number of modifications to GR, e.g., various $f(R)$ gravity models, to elaborate the physics of the different astronomical systems, such as the massive neutron stars (Astashenok et al. 2013, 2014), accretion disk around the compact object (Multamäki and Vilja 2006; Pun et al. 2008; Pérez et al. 2013; Kalita & Mukhopadhyay 2019a), and many more. Our group has also shown that using the suitable forms of $f(R)$ gravity, we can unify the physics of all WDs, including those possessing sub- and super-Chandrasekhar limiting masses (Das & Mukhopadhyay 2015; Kalita & Mukhopadhyay 2018). We showed that by fixing the parameters in a viable $f(R)$ gravity model such that it satisfies the solar system test (Guo 2014), one can obtain the sub-Chandrasekhar limiting-mass WDs at a relatively low density and super-Chandrasekhar WDs at high density (Kalita & Mukhopadhyay 2018). Of course, the mass-radius relation alters from Chandrasekhar's original mass-radius relation depending on the form of $f(R)$ gravity model. Nevertheless, from the recent detection of GW through LIGO/Virgo detectors, researchers have put constraints on the $f(R)$ gravity theory (Vainio & Vilja 2017; Jana & Mohanty 2019).

It is important to note that all the inferences of sub- and super-Chandrasekhar limiting-mass WDs were made indirectly from the luminosity observations of SNe Ia. There is, so far, no direct detection of super-Chandrasekhar WDs in any electromagnetic surveys such as Gaia, Kepler, Sloan Digital Sky Survey, or Wide-field Infrared Survey Explorer, as the massive WDs are usually less luminous compared to the lighter ones (Bhattacharya et al. 2018; Gupta et al. 2020). Therefore, the exact sizes of these peculiar WDs are unknown, and hence nobody could, so far, single out the exact theory of gravity from the various probable models. On the other hand, recent detection of GWs from the merger events opens a new window in astronomy. Since a strong magnetic field and high rotation can increase the mass of a WD, such a WD, possessing a specific configuration, can emit GW efficiently (Kalita & Mukhopadhyay 2019b, 2020; Sousa et al. 2020).

Various advanced futuristic GW detectors such as LISA, DECIGO, and BBO can detect this gravitational radiation for a long time, depending on the field geometry and its strength (Kalita et al. 2020), and thereby one can estimate the size of the super-Chandrasekhar WDs, where the electromagnetic surveys were not successful.

Since $f(R)$ gravity is a better bet to explain and unify all the WDs, including the peculiar ones, to study its validity from observation is extremely necessary. Due to the failure of their direct detections in electromagnetic surveys, GW astronomy seems to be the prominent alternate to detect the peculiar WDs directly. In this way, one can estimate both the mass and the size of the objects, thereby ruling out or putting constraints on the various models of $f(R)$ gravity. Moreover, there is a huge debate on the existence of modifications to GR. Hence, if the futuristic GW detectors such as LISA, ALIA, DECIGO, BBO, or the Einstein Telescope can detect such WDs, it will also be a simple verification for the existence of the modified theories of gravity. We, in this article, present various mechanisms that can produce GWs from $f(R)$ -gravity-induced WDs and discuss how to rule out or single out various theories from such observations.

The article is organized as follows. In Section 2, we discuss the properties of gravitational radiation in $f(R)$ gravity. In Section 3, we discuss the generation of GW from $f(R)$ -gravity-induced WDs through various mechanisms such as the presence of roughness at the surface of WDs, or the presence of magnetic fields and rotation in the WDs. In Section 4, we discuss the amplitude and luminosity of the gravitational radiation emitted from these isolated WDs, and whether the futuristic detector can detect them or not. In Section 5, we discuss the various results and their physical interpretations. In this section, we mainly discuss how to extract information about the WDs from GW detection, and thereby how to put constraints on the modified theories of gravity, before we conclude in Section 6.

2. Gravitational Wave in $f(R)$ Gravity

Assuming the metric signature to be $(-, +, +, +)$ in four dimensions, the action in $f(R)$ gravity (modified Einstein-Hilbert action) is given by (De Felice & Tsujikawa 2010; Will 2014; Nojiri et al. 2017)

$$\mathcal{S}_{f(R)} = \int \left[\frac{c^3}{16\pi G} f(R) + \mathcal{L}_M \right] \sqrt{-g} d^4x, \quad (1)$$

where c is the speed of light, G is Newton's gravitational constant, \mathcal{L}_M is the Lagrangian of the matter field, and $g = \det(g_{\mu\nu})$ is the determinant of the spacetime metric $g_{\mu\nu}$. Varying this action with respect to $g_{\mu\nu}$, with appropriate boundary conditions, we obtain the modified Einstein equation in $f(R)$ gravity, given by

$$F(R)R_{\mu\nu} - \frac{1}{2}g_{\mu\nu}f(R) - (\nabla_\mu\nabla_\nu - g_{\mu\nu}\square)F(R) = \kappa T_{\mu\nu}, \quad (2)$$

where $R_{\mu\nu}$ is the Ricci tensor, $T_{\mu\nu}$ is the matter stress-energy tensor, $F(R) = df(R)/dR$, $\kappa = 8\pi G/c^4$, and \square is the d'Alembertian operator given by $\square = -\partial_t^2/c^2 + \nabla^2$, with ∂_t being the temporal partial derivative and ∇^2 being the three-dimensional Laplacian. For $f(R) = R$, it is obvious that Equation (2) will reduce to the field equation in GR (Ryder 2009). The trace of

Equation (2) is given by

$$RF(R) - 2f(R) + 3 \square F(R) = \kappa g^{\mu\nu} T_{\mu\nu} = \kappa T. \quad (3)$$

Since we plan to explore $f(R)$ gravity models, which can explain both the sub- and super-Chandrasekhar limiting-mass WDs together, the first higher-order correction to GR, i.e., $f(R) = R + \alpha R^2$, seems to suffice for this purpose. However, in this model, one needs to vary the model parameter α to obtain both the regimes of the WDs (Das & Mukhopadhyay 2015), and hence this is probably not the best model for this purpose. Therefore, we need to consider the next higher-order correction terms, i.e., $f(R) = R + \alpha R^2 \{1 - \gamma R + \mathcal{O}(R^2)\}$ (Kalita & Mukhopadhyay 2018), to remove the deficiency of the previous model. In this model, one does not need to vary the parameters α and γ present in the model. Rather, one needs to fix them from the Gravity Probe B experiment, and then, just changing the central density, one can obtain both the sub- and super-Chandrasekhar limiting-mass WDs. Kalita & Mukhopadhyay (2018) provided a detailed analysis of this considering various higher-order corrections to GR and establishing that they still pass the solar system test.

Since we are interested in the most common scenario where GW propagates in vacuum, i.e., in the flat Minkowski spacetime, we need to linearize both $g_{\mu\nu}$ and R . The perturbed forms for $g_{\mu\nu}$ and R are given by

$$g_{\mu\nu} = \eta_{\mu\nu} + h_{\mu\nu}, \quad (4)$$

$$R = R_0 + R_1, \quad (5)$$

with $|h_{\mu\nu}| \ll |\eta_{\mu\nu}|$, where $\eta_{\mu\nu}$ is the background Minkowski metric, R_0 is the unperturbed background scalar curvature, and $h_{\mu\nu}$ and R_1 are, respectively, the tensor and scalar perturbations. Of course, for Minkowski vacuum background, $R_0 = 0$ and $T_0 = 0$, where T_0 is the trace of the background stress-energy tensor. Now perturbing Equations (2) and (3) and substituting the above relations, we obtain the linearized field equations, given by (Capozziello et al. 2008; Liang et al. 2017)

$$\square \bar{h}_{\mu\nu} = -\frac{16\pi G}{c^4} T_{\mu\nu} \quad (6)$$

$$\square h_f - m^2 h_f = \frac{8\pi G}{3F(R_0)c^4} T, \quad (7)$$

where $\bar{h}_{\mu\nu} = h_{\mu\nu} - (h/2 - h_f)\eta_{\mu\nu}$, with $h = \eta_{\mu\nu} h^{\mu\nu}$ and $h_f = F'(R_0)R_1/F(R_0)$. Here m is the effective mass associated with the scalar degree of freedom in $f(R)$ gravity (Sotiriou & Faraoni 2010; Prasia & Kuriakose 2014; Sbisà et al. 2019), given by

$$m^2 = \frac{1}{3} \left\{ \frac{F(R_0)}{F'(R_0)} - R_0 \right\}, \quad (8)$$

where $F' = dF/dR$. Of course, in Minkowski vacuum background, $m^2 = 1/3\{F(0)/F'(0)\}$. It is evident that m depends on the background density, which is known as the chameleon mechanism in $f(R)$ gravity (Burrage & Sakstein 2018; Liu et al. 2018). In Minkowski vacuum background, for $f(R) = R + \alpha R^2(1 - \gamma R)$ with $F(R) = 1 + \alpha R(2 - 3\gamma R)$, Equations (6) and

(7) reduce to

$$\square \bar{h}_{\mu\nu} = -\frac{16\pi G}{c^4} T_{\mu\nu} \quad (9)$$

$$(\square - m^2)R_1 = \frac{4\pi G}{3\alpha c^4} T, \quad (10)$$

with $m^2 = 1/6\alpha$. When the GW propagates in the vacuum, these equations reduce to (Liang et al. 2017; Capozziello et al. 2008)

$$\square \bar{h}_{\mu\nu} = 0, \quad (\square - m^2)R_1 = 0. \quad (11)$$

The first equation is similar to the equation obtained in GR, which means that $\bar{h}_{\mu\nu}$ satisfies the transverse-traceless (TT) gauge condition. This leads to the fact that there is a presence of only two propagating degrees of freedom/polarization for $\bar{h}_{\mu\nu}$ (namely, \bar{h}_+ and \bar{h}_\times). In GR, since $\alpha \rightarrow 0$, or equivalently $m \rightarrow \infty$, only the tensor equation gives the propagating polarization modes. The scalar mode, being infinitely massive in GR, can no longer propagate, and hence the corresponding scalar equation serves as a constraint equation for the tensor modes.¹ On the other hand, in $f(R)$ gravity, since $R \neq 0$ (even in vacuum, due to the presence of R_1), there is the presence of an extra propagating scalar degree of polarization, also known as the breathing mode. Hence, the number of polarizations in $f(R)$ gravity turns out to be 3, unlike the case for GR, where it is 2 (Kausar et al. 2016; Gong & Hou 2018). For a plane wave traveling in the z -direction, the solutions of the above wave Equations (11) are given by

$$\bar{h}_{\mu\nu}(z, t) = \hat{h}_{\mu\nu} \exp[i(\omega z/c - \omega t)], \quad (12)$$

$$R_1(z, t) = \hat{R}_1 \exp[i(\sqrt{\tilde{\omega}^2 - m^2 c^2} z/c - \tilde{\omega} t)], \quad (13)$$

where ω is the frequency of the tensorial modes and $\tilde{\omega}$ is that of the scalar mode. It is evident that the tensorial modes, being massless, propagate at a speed $v_t = c$, whereas the massive scalar mode propagates with a group velocity $v_s = c\sqrt{\tilde{\omega}^2 - m^2 c^2}/\tilde{\omega} < c$ (Yang et al. 2011).

Our aim is to calculate the strength of GW generated from $f(R)$ -gravity-induced WDs. Hence, we need to solve Equations (9) and (10). Since these are inhomogeneous differential equations, we use the method of Green's function. Green's function for the operator $(\square - m^2)$ or $(-\partial_t^2/c^2 + \nabla^2 - m^2)$ is given by (Berry & Gair 2011; Dass & Liberati 2019)

$$\mathcal{G}_m(x, x') = \int \frac{d^4 p}{(2\pi)^4} \frac{\exp[ip \cdot (x - x')]}{m^2 + p^2}, \quad (14)$$

where $p \equiv (\omega/c, \mathbf{k})$, with \mathbf{k} being the wavenumber, such that $p^2 = -\omega^2/c^2 + \mathbf{k}^2$. For a spherically symmetric system with $x \equiv (ct, r = |\mathbf{x} - \mathbf{x}'|, \theta, \phi)$, where \mathbf{x}' and \mathbf{x} are, respectively,

¹ We can also investigate the other extreme regime, i.e., $m \rightarrow 0$ or $\alpha \rightarrow \infty$. From the Gravity Probe B experiment, the bound on α is $|\alpha| \lesssim 5 \times 10^{15} \text{ cm}^2$ (Näf and Jetzer 2010). It is evident that $\alpha \rightarrow \infty$ naturally violates this bound, and hence this limit is unphysical in the present context.

source and observer (detector) positions, it reduces to

$$\mathcal{G}_m(x, x') = \begin{cases} \int \frac{d\omega}{2\pi c} \exp[-i\omega(t-t')] \frac{1}{4\pi r} \exp\left[i\sqrt{\frac{\omega^2}{c^2} - m^2} r\right] & \text{if } \omega^2 > m^2 c^2 \\ \int \frac{d\omega}{2\pi c} \exp[-i\omega(t-t')] \frac{1}{4\pi r} \exp\left[-\sqrt{m^2 - \frac{\omega^2}{c^2}} r\right] & \text{if } \omega^2 < m^2 c^2. \end{cases} \quad (15)$$

Similarly, Green's function for a spherically symmetric \square operator is given by (Berry & Gair 2011)

$$\mathcal{G}_0(x, x') = \frac{\delta(t-t'-r/c)}{4\pi r c}. \quad (16)$$

Therefore, from Equation (9), the solution for $\bar{h}_{\mu\nu}$ is given by

$$\bar{h}_{\mu\nu} = -\frac{4G}{c^4} \int d^3x' \frac{T_{\mu\nu}(t-r, \mathbf{x}')}{r}. \quad (17)$$

Since $\bar{h}_{\mu\nu}$ follows the TT gauge condition like GR, only the space part of the $\bar{h}_{\mu\nu}$ contributes. Assuming the detector to be far from the source such that $x \gg x'$, the above equation reduces to the following form (Ryder 2009):

$$\bar{h}_{ij} = -\frac{2G}{c^4 r} \ddot{Q}_{ij}, \quad (18)$$

where Q_{ij} is the quadrupolar moment of the system with $i, j = 1, 2, 3$. Moreover, from Equation (10), the solution for R_1 is given by

$$R_1 = \frac{4\pi G}{3\alpha c^4} \int d^4x' \mathcal{G}_m(x, x') T(x'). \quad (19)$$

The stress-energy tensor for a perfect fluid is given by

$$T^{\mu\nu} = (\rho c^2 + \mathcal{P})u^\mu u^\nu + \mathcal{P}g^{\mu\nu}, \quad (20)$$

where \mathcal{P} is the pressure, ρ is the density, and u^μ is the four-velocity of the fluid. The trace of $T^{\mu\nu}$ is given by $T = -\rho c^2 + 3\mathcal{P}$. For the case of WD, the equation of state (EoS), known as Chandrasekhar EoS, is governed by the degenerate electron gas. It is given by (Chandrasekhar 1935)

$$\mathcal{P} = \frac{m_e^4 c^5}{24\pi^2 \hbar^3} [x_F(2x_F^2 - 3)\sqrt{x_F^2 + 1} + 3 \sinh^{-1} x_F],$$

$$\rho = \frac{\mu_e m_H (m_e c)^3}{3\pi^2 \hbar^3} x_F^3, \quad (21)$$

where $x_F = p_F/m_e c$, p_F is the Fermi momentum, m_e is the mass of an electron, \hbar is the reduced Planck's constant, μ_e is the mean molecular weight per electron, and m_H is the mass of a hydrogen atom. For our work, we choose $\mu_e = 2$, indicating the carbon-oxygen WDs. It is evident, from this EoS, that $\rho c^2 \gg \mathcal{P}$ and, hence, $T \approx -\rho c^2$. Moreover, from the Gravity Probe B experiment, the bound on α is $|\alpha| \lesssim 5 \times 10^{15} \text{ cm}^2$ (Näf and Jetzer 2010). We already showed in our previous work that $\alpha = 3 \times 10^{14} \text{ cm}^2$ is enough to probe both sub- and super-Chandrasekhar limiting-mass WDs simultaneously (Kalita & Mukhopadhyay 2018). For this value of α , in vacuum background, $m^2 = 1/6\alpha \approx 5.6 \times 10^{-16} \text{ cm}^{-2}$, and hence the cutoff frequency turns out to be $\omega_c = mc \approx 709.5 \text{ rad s}^{-1}$. The

rotation period $\Omega_{\text{rot}} \sim \omega$ of a WD is always $\lesssim 10 \text{ rad s}^{-1}$. Hence, in Equation (15), $\omega^2 \ll m^2 c^2 = \omega_c^2$ is satisfied, and Green's function reduces to (Stabile 2010)

$$\mathcal{G}_m(x, x') = \frac{\delta(t-t')}{4\pi r c} e^{-mr}. \quad (22)$$

Therefore, using Equation (19), for a WD, the solution for R_1 is given by

$$R_1 = \frac{G}{3\alpha c^2} \int d^3x' \frac{\rho(x')}{|x-x'|} e^{-m|x-x'|}. \quad (23)$$

The typical distance of a WD from Earth is $\sim 100 \text{ pc}$ ($1 \text{ pc} \approx 3.1 \times 10^{18} \text{ cm}$), which means $x \gg x'$. Hence, for a WD with mass M , R_1 reduces to

$$R_1 \propto \frac{GM}{3\alpha c^2 r} e^{-mr}. \quad (24)$$

For the chosen values of m and r , $mr \approx 7.3 \times 10^{12}$, which means that the scalar mode's amplitude is exponentially suppressed enormously (Katsuragawa et al. 2019), and the detectors cannot detect them. Hence, in the rest of the article we discuss only the tensorial modes \bar{h}_{ij} given by Equation (18), and for convenience we remove "bar" from h hereinafter.

3. Mechanisms for Generating GW from an Isolated WD

In this section, we discuss a couple of mechanisms that can generate gravitational radiation from an isolated WD. From Equation (18), it is evident that a system can emit gravitational radiation if and only if the system possesses a time-varying quadrupolar moment such that $\dot{Q}_{ij} \neq 0$. Hence, neither a spherically symmetric system nor an axially symmetric system can radiate GW, and a triaxial system is required. In a triaxial system, the moment of inertia is different along all three spatially perpendicular axes. There are mainly two ways by which a WD can be triaxial (Shapiro & Teukolsky 1983). First, the rotating WD already possesses roughness at its surface, perhaps due to the presence of mountains and holes (craters). The second possibility is that the WD possesses the magnetic field and rotation, with a nonzero angle between their respective axes. We now discuss each of these possibilities one by one.

3.1. GW due to Roughness of the Surface

If a WD possesses asymmetry of matter at its surface, the moments of inertia of the WD are different along all directions, making the system a triaxial one. If such a WD rotates with angular velocity Ω_{rot} , it can emit effective gravitational radiation continuously. Suppose the moments of inertia for such a system are I_1, I_2 , and I_3 along the x -, y -, and z -axes, respectively, such that $I_1 < I_2 < I_3$. Thereby, using Equation (18), the two tensorial polarizations of GW, at time t , are given by (Zimmermann 1980; Van Den Broeck 2005; Maggiore 2008)

$$h_+ = A_{+,0} \cos(2\Omega_{\text{rot}} t) + A_{+,1} \cos[(\Omega_{\text{rot}} + \Omega_p)t] \\ + A_{+,2} \cos[2(\Omega_{\text{rot}} + \Omega_p)t],$$

$$h_\times = A_{\times,0} \sin(2\Omega_{\text{rot}} t) + A_{\times,1} \sin[(\Omega_{\text{rot}} + \Omega_p)t] \\ + A_{\times,2} \sin[2(\Omega_{\text{rot}} + \Omega_p)t], \quad (25)$$

where

$$\begin{aligned}
A_{+,0} &= (h_0/2)(1 + \cos^2 i), \\
A_{+,1} &= 2h_0'(I_1 a/I_3 b) \sin i \cos i, \\
A_{+,2} &= 2h_0'(I_1 a/I_3 b)^2(1 + \cos^2 i), \\
A_{\times,0} &= h_0 \cos i, \\
A_{\times,1} &= 2h_0'(I_1 a/I_3 b) \sin i, \\
A_{\times,2} &= 4h_0'(I_1 a/I_3 b)^2 \cos i,
\end{aligned} \tag{26}$$

with i being the inclination angle between the rotation axis of the WD and the detector's line of sight, and

$$\begin{aligned}
h_0 &= -\frac{4G\Omega_{\text{rot}}^2 I_3}{rc^4} \left(\frac{I_1 - I_2}{I_3} \right), \\
h_0' &= -\frac{G(\Omega_{\text{rot}} + \Omega_p)^2 I_3}{rc^4} \left(1 - \frac{I_1 + I_2}{2I_3} \right).
\end{aligned} \tag{27}$$

Here a and b are given by

$$a = \sqrt{\frac{2\tilde{E}I_3 - \tilde{M}^2}{I_1(I_3 - I_1)}}, \quad b = \sqrt{\frac{\tilde{M}^2 - 2\tilde{E}I_1}{I_3(I_3 - I_1)}}, \tag{28}$$

where $\tilde{E} = (I_1\Omega_1^2 + I_2\Omega_2^2 + I_3\Omega_3^2)/2$ and $\tilde{M}^2 = I_1^2\Omega_1^2 + I_2^2\Omega_2^2 + I_3^2\Omega_3^2$, with Ω_1, Ω_2 , and Ω_3 being the components of initial angular velocity along x -, y -, and z -axes, respectively (Landau & Lifshitz 1982). The precession frequency is given by

$$\Omega_p = \frac{\pi b}{2K(\tilde{m})} \left[\frac{(I_3 - I_2)(I_3 - I_1)}{I_1 I_2} \right]^{1/2}, \tag{29}$$

where $K(\tilde{m})$ is the complete elliptic integral of the first kind, with the ellipticity parameter \tilde{m} given by

$$\tilde{m} = \frac{(I_2 - I_1)I_1 a^2}{(I_3 - I_2)I_3 b^2}. \tag{30}$$

The rotation frequency is given by

$$\begin{aligned}
\Omega_{\text{rot}} &= \frac{\tilde{M}}{I_1} + \frac{2b}{K(\tilde{m})} \left[\frac{(I_3 - I_2)(I_3 - I_1)}{I_1 I_2} \right]^{1/2} \\
&\times \sum_{n=1}^{\infty} \frac{q^n}{1 - q^{2n}} \sinh(2\pi n c_1) - \Omega_p,
\end{aligned} \tag{31}$$

where $q = \exp\{-\pi K(1 - \tilde{m})/K(\tilde{m})\}$, and c_1 satisfies:

$$\text{sn}[2ic_1 K(\tilde{m}), \tilde{m}] = i \frac{I_3 b}{I_1 a}. \tag{32}$$

It is evident from the set of Equations (25) that for a triaxial system GW is associated with three frequencies, which implies that one should expect three distinct lines in the spectrum. In reality, not only three in the spectrum but also lines with higher frequencies, arising from higher-order terms, may also be present, but their intensities are suppressed (Maggiore 2008).

3.2. GW due to Breaking of Axial Symmetry through Rotation

One more possibility of generating GWs from an isolated WD is by breaking the preexisting axial symmetry through rotation. A WD can be axially symmetric if it possesses a magnetic field (either toroidal or poloidal or any other suitable mixed field configuration). Now, if the WD rotates with a

misalignment between its rotation and magnetic axes (similar configuration to a neutron star pulsar), it can emit gravitational radiation continuously. For such an object, with χ being the angle between the magnetic field and rotation axes, using Equation (18), the two tensorial polarizations of GWs are given by (Zimmermann & Szedenis 1979; Bonazzola & Gourgoulhon 1996)

$$\begin{aligned}
h_+ &= \tilde{A}_{+,1} \cos(\Omega_{\text{rot}} t) - \tilde{A}_{+,2} \cos(2\Omega_{\text{rot}} t), \\
h_{\times} &= \tilde{A}_{\times,1} \sin(\Omega_{\text{rot}} t) - \tilde{A}_{\times,2} \sin(2\Omega_{\text{rot}} t),
\end{aligned} \tag{33}$$

where

$$\begin{aligned}
\tilde{A}_{+,1} &= \tilde{h}_0 \sin 2\chi \sin i \cos i, \\
\tilde{A}_{+,2} &= 2\tilde{h}_0 \sin^2 \chi (1 + \cos^2 i), \\
\tilde{A}_{\times,1} &= \tilde{h}_0 \sin 2\chi \sin i, \\
\tilde{A}_{\times,2} &= 4\tilde{h}_0 \sin^2 \chi \cos i,
\end{aligned} \tag{34}$$

with

$$\tilde{h}_0 = \frac{G}{c^4} \frac{\Omega_{\text{rot}}^2 (I_3 - I_1)}{r}. \tag{35}$$

Hence, in this configuration, a continuous GW is emitted at two frequencies, namely, Ω_{rot} and $2\Omega_{\text{rot}}$.

4. Strength of GW Emitted from an Isolated WD

In this section, we discuss the strength of GWs emitted from an $f(R)$ -gravity-induced isolated WD. We earlier showed that in the presence of $f(R)$ gravity with $f(R) = R + \alpha R^2(1 - \gamma R)$, where $\alpha = 3 \times 10^{14} \text{ cm}^2$ and $\gamma = 4 \times 10^{16} \text{ cm}^2$, it is possible to obtain sub-Chandrasekhar limiting-mass WDs, as well as super-Chandrasekhar WDs, along with the regular WDs just varying the central density ρ_c of the WDs (Kalita & Mukhopadhyay 2018). We also showed that, with the chosen values of the parameters, this model is valid in terms of the solar system test (Guo 2014). For demonstration, we recall the key results from that work, depicted in Figure 1, which shows the variation of radius \mathcal{R} and ρ_c with respect to M . WDs following GR are shown with the green dashed line, and the red solid line corresponds to the $f(R)$ -gravity-induced WDs. Indeed, there are some WDs, e.g., EG 50, GD 140, J2056-3014, etc. (Provencal et al. 1998; Lopes de Oliveira et al. 2020), that do not follow the standard Chandrasekhar mass-radius relation. Moreover, it is to be noted that we adopt the perturbative calculations and consider the exterior solution of the WD to be the Schwarzschild solution while obtaining the mass-radius curve in $f(R)$ gravity. As a result, R is asymptotically flat outside the WD (Ganguly et al. 2014; Capozziello et al. 2016). Moreover, in perturbative analysis, a WD is unstable under the radial perturbation if it falls in the branch where $\partial M/\partial \rho_c < 0$ ($\partial M/\partial \rho_c > 0$ is known as the positivity condition, which is a necessary condition for stability; Shapiro & Teukolsky 1983; Glendenning 2010). In perturbative method, while obtaining the mass-radius curve, $\partial M/\partial \rho_c > 0$ still defines the stability criterion like GR, because any additional terms will be just perturbative corrections to the zeroth-order quantity, which are usually small. From the figure, we observe that at low ρ_c the effect of modified gravity is negligible, as both curves overlap with each other (mostly in the branch AB). As ρ_c increases, the mass-radius curve reaches a maximum at the mass $\sim M_{\odot}$ and $\rho_c \sim 1.5 \times 10^8 \text{ g cm}^{-3}$ (point B). Beyond this ρ_c , the curve turns back, which violates the positivity condition, and hence BC is an

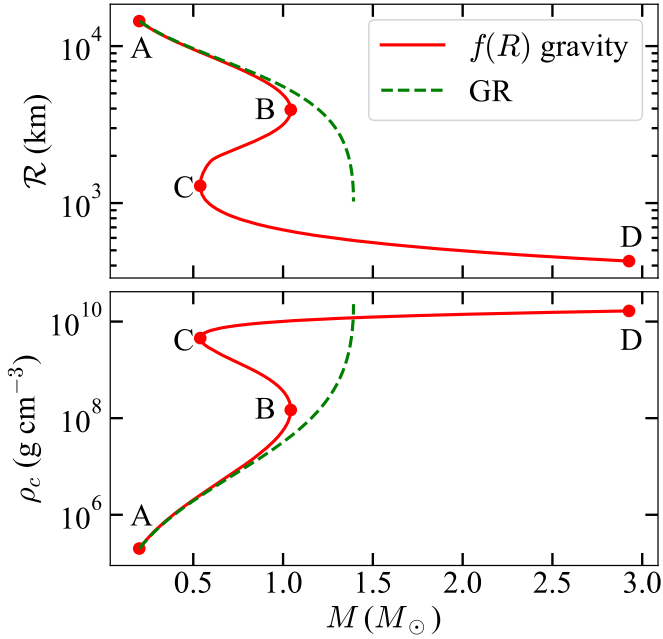


Figure 1. Variation of radius and central density with respect to the mass of the WD.

unstable branch. Therefore, point B corresponds to the sub-Chandrasekhar limiting-mass WD. Further, reaching a minimum value, the curve again turns back from point C and quickly enters in the super-Chandrasekhar WD regime following $\partial M/\partial \rho_c > 0$. Since the branch CD is stable, the super-Chandrasekhar WDs are stable under radial perturbation. The maximum ρ_c is chosen in such a way that it does not violate any of the known physics for CO WDs, such as neutron drip (Shapiro & Teukolsky 1983), pycno-nuclear reactions and inverse beta decay (Otoniel et al. 2019), etc. The empirical relation between \mathcal{R} and M in the branch AB is approximately $\mathcal{R} \propto M^{-2/5}$, that in the branch BC is $\mathcal{R} \propto M$, and that in the branch CD is $\mathcal{R} \propto M^{-1/2}$. In this way, this form of $f(R)$ gravity, with the chosen parameters, can explain both the sub- and super-Chandrasekhar limiting-mass WDs just by varying the ρ_c . It is, however, evident that there is no super-Chandrasekhar mass limit in this model. Such a mass limit is possible if we consider higher-order corrections (at least 16th order) to the Starobinsky model as discussed earlier (Kalita & Mukhopadhyay 2018). The beauty of this model is that at the low-density limit the extra terms of modified gravity have a negligible effect, and GR is enough to describe the underlying physics. In the case of a star, its density is relatively small compared to the WD’s density, and hence, even if the same α and γ remain intact, their effect is not prominent in the star phase. It has a significant effect only when the star becomes a WD depending on the density. Now, based on this mass–radius relation, we discuss the corresponding strength of GWs separately for each of the possibilities, mentioned in the previous section.

4.1. Presence of Roughness at WD’s Surface

We have already mentioned that if a preexisting triaxial WD rotates, it can produce continuous gravitational radiation. One possibility for a WD being triaxial is due to the asymmetry of matter present at its surface. One can imagine this configuration as a similar structure of Earth or the Moon, where there are mountains and craters (holes) at the surface. We assume that there are excess “mountains” along the x -axis and “holes”

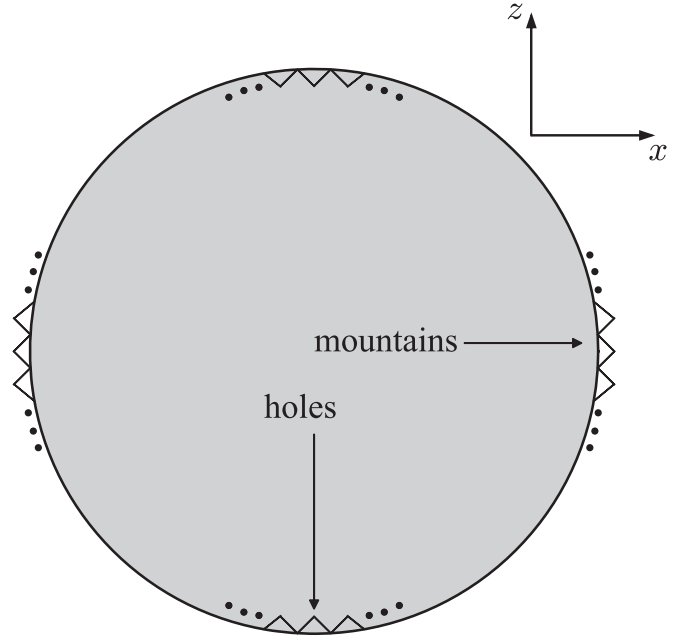


Figure 2. Exaggerated figure of the presence of mountains and holes at the surface of a WD.

along the z -axis of a WD, as shown in Figure 2. Such a configuration guarantees a triaxial system with $I_1 < I_2 < I_3$. For simplicity, we assume $\Omega_1 = \Omega_2 = \Omega_3$.

Let us now check the maximum possible height of a mountain on a WD’s surface. Assuming the mountains to be generated as a result of the shear in the outer envelope of WDs (same as the case for Earth, where there are mountains at its crust), the maximum height of a mountain is given by (Sedrakian et al. 2005)

$$H = \frac{S}{\rho g}, \quad (36)$$

where ρ is the average density of the mountain, g is the acceleration due to gravity at the surface of the WD, and S is the shear modulus, which is given by (Mott & Jones 1958; Baym & Pines 1971)

$$S = 0.295 Z^2 e^2 n_e^4 / 3, \quad (37)$$

with e being the charge of an electron, Z the atomic number, and n_e the electron number density in the mountain. Substituting this expression, the maximum height of the mountain reduces to

$$H = 3.637 \times 10^{12} \frac{Z^2}{g} \rho^{1/3} \text{ cm}. \quad (38)$$

Assuming the C-O WDs with the surface mostly consisting of He, we choose $Z=2$. Moreover, assuming the mountains’ average density to be the density just below the surface of the WDs, i.e., $\rho \approx 10^{-6} \rho_c$, we obtain H for various WDs with different values of ρ_c , which is shown in Figure 3. From the empirical relations mentioned in the previous section, we also obtain the same between H and M : in the branch AB, $H \propto M^{-2/5}$, in CD, $H \propto M^{-7/6}$, while in BC, H is nearly constant.

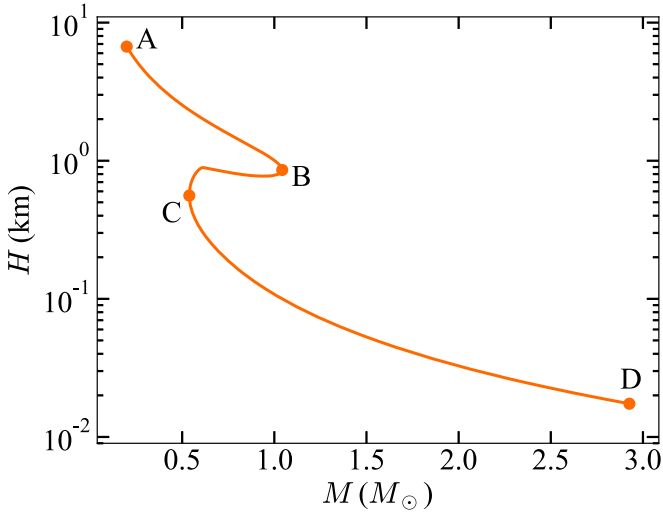


Figure 3. Maximum height of a mountain present on a WD as a function of mass.

It is evident from Figure 3 that $H \ll \mathcal{R}$. However, if there are a series of mountains of similar heights on the x -direction and big holes on the z -direction, as shown in Figure 2, effective radii of the WDs change. The effective radii in x -, y -, and z -directions become $\mathcal{R} + H$, \mathcal{R} , and $\mathcal{R} - H$, respectively, resulting in a triaxial system. Hence, the moments of inertia along different directions are given by

$$\begin{aligned} I_1 &= \frac{M}{5} [\mathcal{R}^2 + (\mathcal{R} - H)^2], \\ I_2 &= \frac{M}{5} [(\mathcal{R} + H)^2 + (\mathcal{R} - H)^2], \\ I_3 &= \frac{M}{5} [\mathcal{R}^2 + (\mathcal{R} + H)^2]. \end{aligned} \quad (39)$$

Moreover, we know that rotation can also increase the mass and radius of a WD. Hence, we assume the angular frequency to be 1/10 of the maximum possible angular frequency, i.e., $\Omega = 1/10 \sqrt{GM/\mathcal{R}^3}$, such that it does not affect the mass and size of the WD. Using the set of Equations (26), we obtain the dimensionless strain amplitude of GW, A (e.g., $A_{+,0}$, $A_{\times,0}$, etc.), emitted from WDs with a rough surface, corresponding to all three frequencies of the spectrum. Moreover, we know that the integrated signal-to-noise ratio (S/N) increases if we observe the source for a long period of time \mathcal{T} . The relation between S/N and \mathcal{T} is given by (Maggiore 2008; Thrane & Romano 2013; Sieniawska & Bejger 2019)

$$\text{S/N} = \frac{1}{\sqrt{5}} \left(\frac{\mathcal{T}}{S(\nu)} \right)^{1/2} A, \quad (40)$$

where $S(\nu)$ is the power spectral density (PSD) at a frequency ν . We show the PSD of various detectors as a function of frequency² (Sathyaprakash & Schutz 2009; Moore et al. 2015) in Figure 4, along with $\sqrt{\mathcal{T}/5}A$ for $f(R)$ -gravity-induced WDs with $\rho_c = 10^6, 10^7, 10^8, 10^9, 10^{10}$, and $1.66 \times 10^{10} \text{ g cm}^{-3}$ over $\mathcal{T} = 5 \text{ s}$ assuming $r = 100 \text{ pc}$. It is evident that many of these dense WDs will readily, or at most in a few seconds, be

detected by DECIGO and BBO with $\text{S/N} \gtrsim 5$. Since the signal is continuously emitted for a long duration, the significantly super-Chandrasekhar WDs, being smaller in size, can also be detected by the Einstein Telescope with $\text{S/N} \approx 5$ if the signal is integrated over $\mathcal{T} \sim 102$ minutes. However, to detect these WDs by ALIA or LISA with the same S/N, the integration time turns out to be $\mathcal{T} \sim 3$ months and $\mathcal{T} \sim 40,000 \text{ yr}$, respectively. Hence, it seems impossible for LISA to detect the GW signal from WDs with rough surfaces. Figure 5(a) shows $\sqrt{\mathcal{T}/5}A$ for different integration times for these WDs. It is evident from this figure that S/N increases as the integration time increases, allowing the possibility of detecting these WDs even by the Einstein Telescope and ALIA. Furthermore, due to the emission of gravitational radiation, it is associated with the quadrupolar luminosity, given by (Zimmermann 1980)

$$\begin{aligned} L_{\text{GW}} &= -dE/dt = -I_3 \Omega_{\text{rot}} \dot{\Omega}_{\text{rot}} \\ &\approx \frac{32G}{5c^5} b^6 (I_2 - I_1)^2 + \frac{2G}{5c^5} a^2 b^4 \left(I_3 - \frac{I_1 + I_2}{2} \right)^2. \end{aligned} \quad (41)$$

Since there is no magnetic field in this WD configuration, there will be no associated electromagnetic counterpart. In other words, these WDs do not emit any dipole radiation. Nevertheless, due to the emission of GW radiation, the WD starts spinning down, i.e., Ω_{rot} decreases with time. After a certain period of time (characteristic timescale, P , of a WD pulsar), it will lose all its rotational energy and can no longer radiate any gravitational radiation. Using the expression for L_{GW} , we obtain

$$P \approx \frac{135 I_3 c^5}{2G \Omega_{\text{rot}}^4} \frac{1}{64 Y^3 (I_2 - I_1)^2 + X Y^2 (2I_3 - I_1 - I_2)^2}, \quad (42)$$

with

$$X = 1 + \frac{I_2 (I_3 - I_2)}{I_1 (I_3 - I_1)} \quad \text{and} \quad Y = 1 + \frac{I_2 (I_2 - I_1)}{I_3 (I_3 - I_1)}.$$

Figure 6 shows the variation of L_{GW} and P with respect to M of WD. The empirical relations for L_{GW} and P in various branches are given in Table 1. It is evident that the lifetime of massive WD pulsars is shorter than that of the lighter WDs.

4.2. Presence of Magnetic Field in WD

As mentioned in the previous section, if a magnetized WD rotates with a misalignment between its magnetic field and rotation axes (similar configuration to a pulsar), it can emit a continuous GW. We already provided a detailed discussion on GWs emitted from WDs with different magnetic field geometries and strengths in GR (Kalita & Mukhopadhyay 2019b; Kalita et al. 2020). Figure 7 shows an illustrative diagram of a magnetized WD where the magnetic field is along the z' -axis and rotation is along the z -axis, with χ being the angle between these two axes. We calculate the amplitude of GW using the set of Equations (34) assuming the difference in radii of the WD between those along x - and z -axes to be 0.01%, i.e., $\epsilon = |I_3 - I_1|/I_3 \approx 2 \times 10^{-4}$, due to the presence of a very weak magnetic field and slow rotation. The choice of weak fields and slow rotation assures that the underlying WD mass–radius solutions do not practically differ from the solutions based on the $f(R)$ gravity without magnetic fields and

² <http://gwplotter.com/>

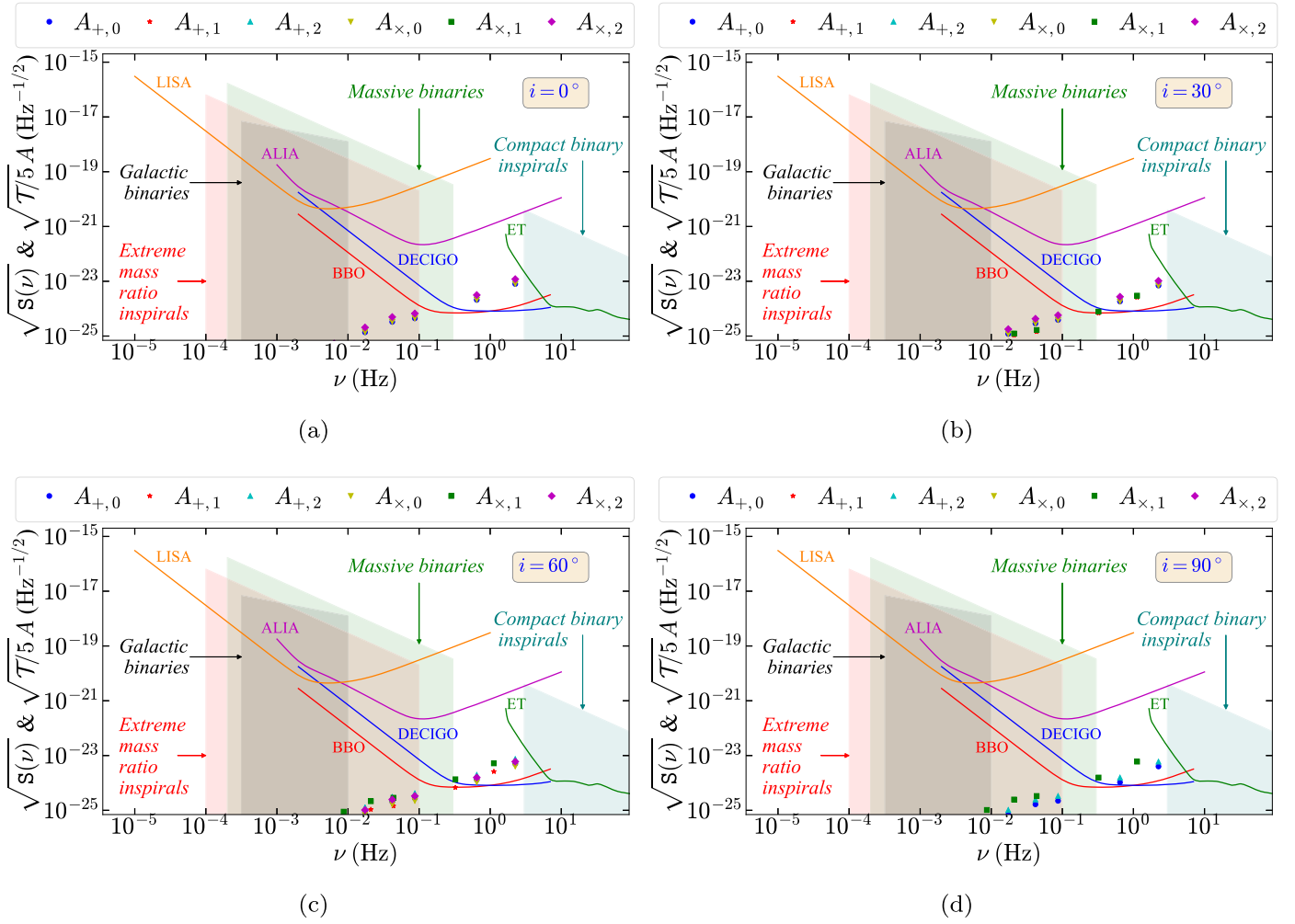


Figure 4. $\sqrt{T/5}A$ for $f(R)$ -gravity-induced WDs with rough surfaces for different i over 5 s integration time along with various detectors' PSD.

rotation. In future, we plan to check rigorously by solving the set of equations, if indeed such ϵ is possible in the presence of weak magnetic fields and rotation keeping the mass and radius practically intact. As we will show below, however, the chosen ϵ appears to be the minimally required value to have any appreciable effect. Nevertheless, there are examples of weakly magnetized WD pulsars, which can be explained even in the GR framework, e.g., AE Aquarii (Bookbinder & Lamb 1987) and AR Scorpii (Marsh et al. 2016), where magnetic fields hardly affect their mass–radius relations. Figure 8 shows the PSD as a function of frequency for various detectors along with $\sqrt{T/5}A$ over 5 s integration time for various $f(R)$ -gravity-induced WD pulsars with different i assuming $\chi = 90^\circ$ and $r = 100$ pc. It is evident that while DECIGO and BBO can immediately detect such weakly magnetized super-Chandrasekhar WDs, the Einstein Telescope can detect them in $\mathcal{T} \sim 6$ minutes with $S/N \approx 5$ (see Figure 5(b)). However, for ALIA and LISA, the corresponding integration time respectively turns out to be $\mathcal{T} \sim 5$ days and $\mathcal{T} \sim 25,000$ yr³. Hence, it is also possible to detect such weakly magnetized WDs using ALIA, whereas for LISA it is quite impossible. Figure 5(b) depicts $\sqrt{T/5}A$ for these WDs with different integration times to show that S/N increases if the integration

³ Note that even if the threshold S/N for detection increases slightly (say, from 5 to 20), many of these sources can still be detected in a few seconds to a few days of integration time depending on the type of the detectors.

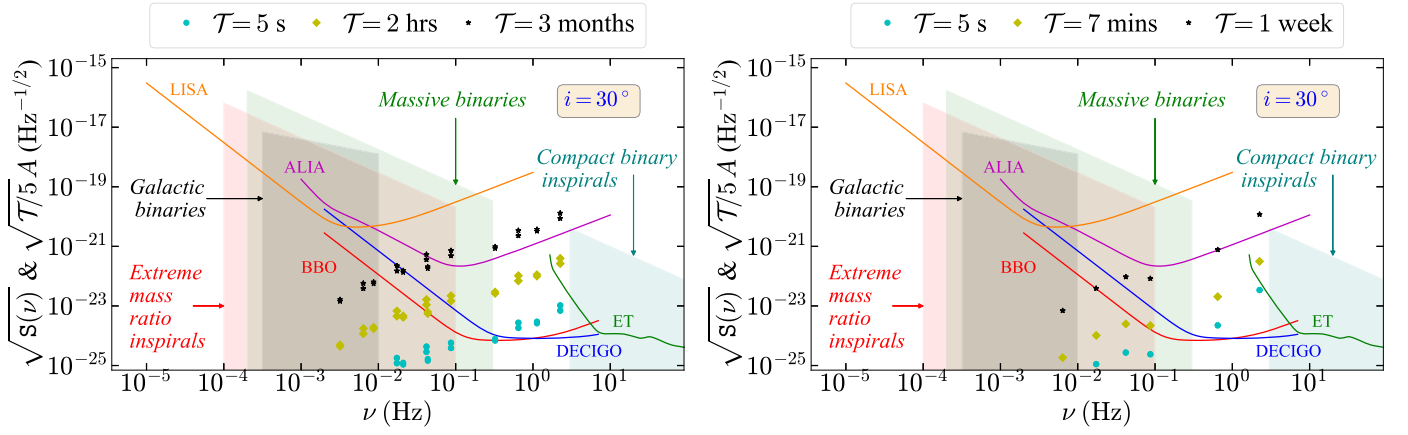
time increases so that various detectors can detect them eventually. For such a system, the GW luminosity is given by (Zimmermann & Szedenits 1979)

$$L_{\text{GW}} \approx \frac{2G}{5c^5} (I_3 - I_1)^2 \Omega^6 \sin^2 \chi (1 + 15 \sin^2 \chi). \quad (43)$$

It is expected that a source can emit electromagnetic radiation in the presence of a magnetic field, and it is the dipole radiation in the case of a WD pulsar. However, because of the presence of a weak magnetic field, the dipole radiation emitted from such a WD is minimal, and the corresponding dipole luminosity is negligible as compared to L_{GW} . Hence, the spin-down timescale is mostly governed by L_{GW} , given by (Kalita et al. 2020)

$$P \approx \left(\frac{5I_3 c^5}{8G(I_3 - I_1)^2 \Omega^4} \right) \frac{1}{\sin^2 \chi (1 + 15 \sin^2 \chi)}. \quad (44)$$

Figure 9 shows the variation of L_{GW} and P with respect to M for various WDs with $\chi = 90^\circ$. The maximum L_{GW} in the case of a WD is $\sim 10^{37}$ erg s⁻¹. The empirical relations of L_{GW} and P , in various branches, are same as in the previous case provided in Table 1. It is also clear from the figure that the massive WD pulsars are short-lived as compared to the lighter ones.



(a) WDs with surface roughness.

(b) WDs with magnetic field.

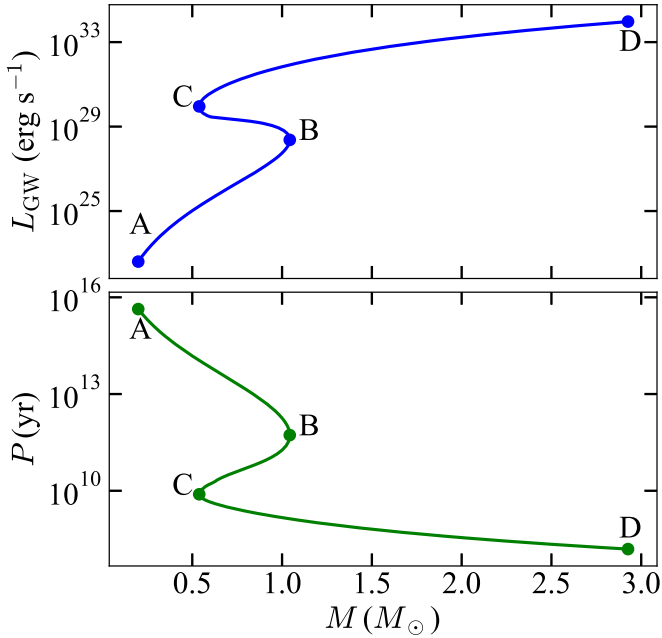
Figure 5. $\sqrt{T/5 A}$ for $f(R)$ -gravity-induced WDs with $i = 30^\circ$ and different integration time along with various detectors' PSD.

Figure 6. Variation of L_{GW} and P with respect to the mass of WD with mountains and holes.

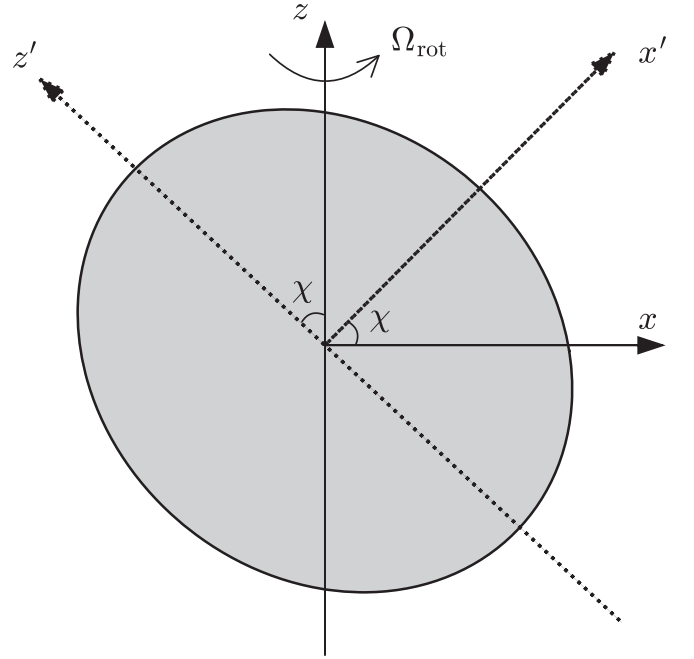
Table 1

Empirical Relations of Various Quantities with Respect to Mass of the WDs

Quantity	AB Branch	BC Branch	CD Branch
Radius	$\mathcal{R} \propto M^{-2/5}$	$\mathcal{R} \propto M$	$\mathcal{R} \propto M^{-1/2}$
Maximum height	$H \propto M^{-2/5}$	$H \approx \text{constant}$	$H \propto M^{-7/6}$
Luminosity	$L_{\text{GW}} \propto M^3$	$L_{\text{GW}} \approx \text{constant}$	$L_{\text{GW}} \propto M^{5/2}$
Timescale	$P \propto M^{-23/5}$	$P \propto M$	$P \propto M^{-5}$

5. Discussion

From Figures 4 and 8, we observe that the GW frequency of isolated WDs could be much larger as compared to that of galactic binaries. This is because, in the case of isolated WDs, the spin frequency is responsible for the GW generation, whereas, in the case of binaries their orbital periods are essential. Therefore, the confusion noise of the binaries does not affect the detection of


Figure 7. Cartoon diagram of a magnetized WD with magnetic field along the z' -axis and rotation along the z -axis.

the isolated WDs. However, the GW frequency of some other sources, such as massive binaries and compact binary inspirals, is similar to that of isolated WDs. Hence, using specific templates for binaries, the objects can be distinguished from each other. Of course, the frequency range of isolated WDs is such that neither the nanohertz detectors, such as IPTA, EPTA, and NANOGrav, nor the other currently operating ground-based detectors, such as LIGO, VIRGO, and KAGRA, can detect them.

From Figure 1, it is evident that the GR-dominated WDs are considerably big as compared to the $f(R)$ -gravity-dominated ones, particularly at higher central densities, provided they possess the same central density. Moreover, using Equations (27) and (35), we have $h_0 \propto I$, with I being the typical moment of inertia of the body. As a result, if we compare two WDs with the same ellipticity and angular frequency, the GR-dominated WD emits stronger gravitational radiation. Since this paper is dedicated to studying the effect of $f(R)$ gravity, we do not explicitly calculate

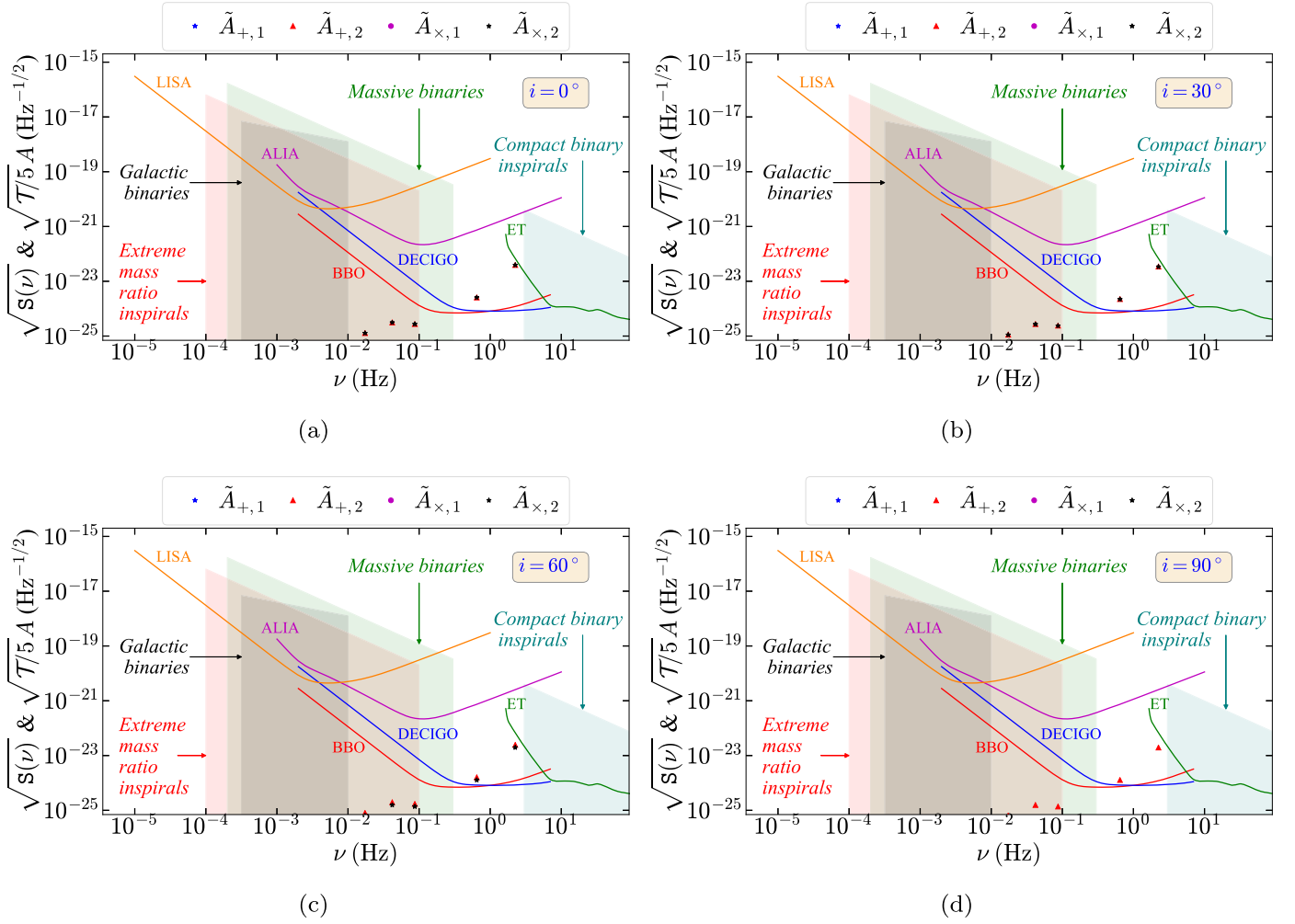


Figure 8. $\sqrt{T/5}A$ for $f(R)$ -gravity-induced weakly magnetized WD pulsars for different i over 5 s integration time along with various detectors' PSD.

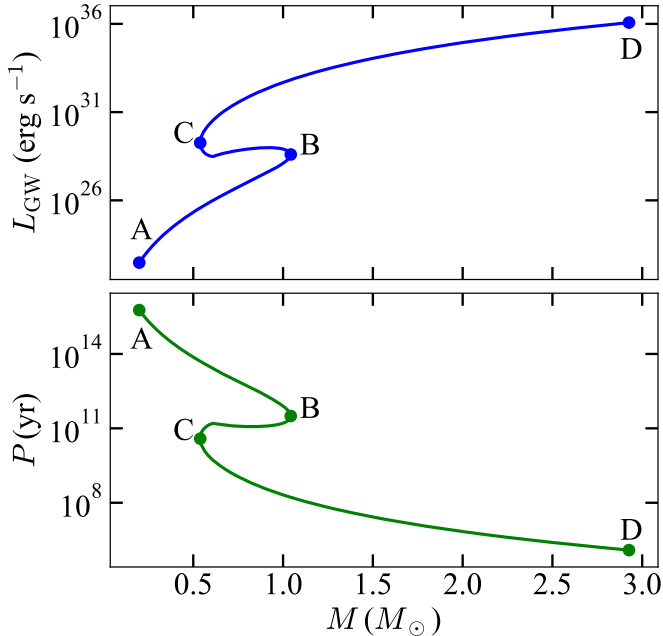


Figure 9. Same as Figure 6, except that the WDs have magnetic field instead of mountains.

h_0 in the case of GR, like we have calculated it in detail in our earlier papers (Kalita & Mukhopadhyay 2019b, 2020; Kalita et al. 2020). Moreover, we focus on exploring the detectability of those WDs that exhibit sub- and super-Chandrasekhar limiting-mass WDs in the same M - \mathcal{R} relation, which GR-based theory cannot, and it has many consequences outlined in the Introduction. However, it is to be noted that $f(R)$ -gravity-dominated WDs, being smaller in size, can rotate much faster with frequency $\gtrsim 1$ Hz, which is not possible in the case of a regular WD governed by GR. In this paper, we have shown that in the presence of small deformation, such as the presence of a rough surface or magnetic fields, these WDs can emit intense gravitational radiation, which can later possibly be detected by BBO, DECIGO, ALIA, and the Einstein Telescope.

The birth rate of He-dominated WDs is $\sim 1.5 \times 10^{-12} \text{ pc}^{-3} \text{ yr}^{-1}$ (Guseinov et al. 1983), which means that within 100 pc radius only one WD is formed in approximately 10^6 yr. Hence, continuous GWs from some massive WDs, which have radiation timescales (life span) $\sim 10^{8-9}$ yr, can be detected, as shown in Figures 4 and 8. If the advanced futuristic detectors, such as DECIGO, BBO, or the Einstein Telescope, detect the isolated WDs, one can quickly check whether the physics is governed by GR, or $f(R)$ gravity, or any other modified theory of gravity as follows. Once the GW detectors detect such a WD, we have the information of h_0 and Ω_{rot} . Consequently, if the distance to the source r is known by

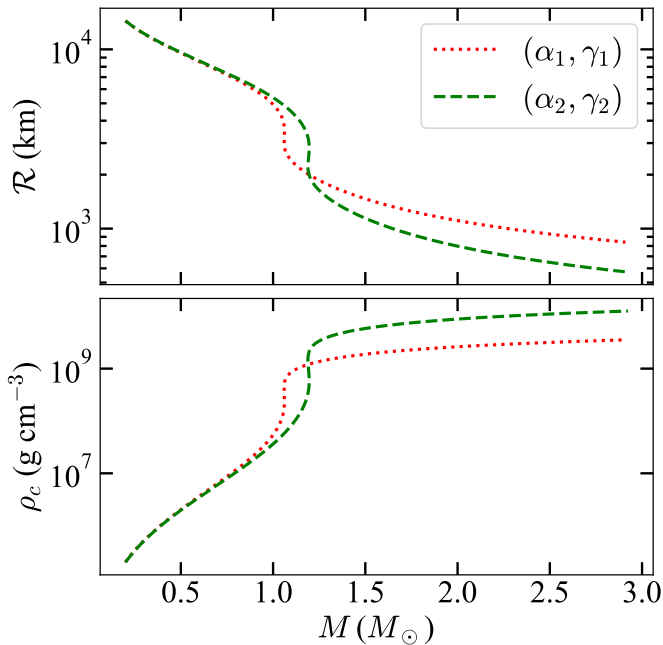


Figure 10. M - R and M - ρ_c relations for WDs for the $f(R) = R + \alpha R^2(1 - \gamma R)$ model. The values of α and γ in the units of cm^2 are $(\alpha_1, \gamma_1) = (10^{14}, 10^{17})$ and $(\alpha_2, \gamma_2) = (3 \times 10^{14}, 3 \times 10^{17})$.

some other method, then, by using Equations (27) and (35), one can estimate the ellipticity and thereby can predict the mass and size of the WD. This will be a direct detection of the WD with low thermal luminosity (usually a super-Chandrasekhar WD that is smaller in size). In this way, we obtain the exact mass–radius relation of the WD. Since different theories provide different mass–radius relations of the WD, by obtaining the exact mass–radius relation from observation, one can rule out various theories from the zoo of modified theories of gravity that do not follow this relation. For example, Figure 10 shows mass–radius relations for a particular $f(R)$ gravity model but with different sets of model parameters. Comparing these results with those shown in Figure 1 reveals that the range of radius for stable WDs depends on the chosen model parameters for the same ranges of mass and central density. Direct detection of the WDs will provide valuable information to identify the correct radius range and hence mass–radius relation of the WDs.

6. Conclusions

In this paper, we have established a link between theory and possible GW observations of the WDs in an $f(R)$ gravity. Various researchers have already proposed hundreds of modified theories of gravity, including many $f(R)$ gravity theories, and each one of them possesses its own peculiarity. However, because of the lack of advanced observations near the extremely high gravity regime, nobody, so far, can rule out most of the models to single out one specific theory of gravity. In this paper, we consider one valid class of $f(R)$ gravity model from the solar system constraints, which can explain both the sub- and super-Chandrasekhar WDs, along with the normal WDs, depending only on their central densities and keeping the parameters of the model fixed. However, from the point of observation, the primary difficulty is that we do not know the size of the peculiar WDs and, hence, the exact mass–radius curve is still unknown. Thereafter, we calculate the strength of GWs emitted from these WDs, assuming they slowly rotate

with little deformation due to some other factors, such as the presence of roughness of the envelope, or the presence of a weak magnetic field. If the advanced futuristic GW detectors, such as ALIA, DECIGO, BBO, or the Einstein Telescope, can detect these WDs, one can estimate the ellipticity of the WDs and thereby put bounds on the WD’s size. This will restrict the mass–radius relation of the WD, which can rule out various modified theories, and we will be inching toward the ultimate theory of gravity.

The authors would like to thank Clifford M. Will of the University of Florida for his insightful comments on the effect of modified gravity in triaxial systems. S.K. would also like to thank Khun Sang Phukon of Nikhef, Amsterdam, for the useful discussions on integrated S/N in the case of various detectors. Finally, thanks are due to the anonymous referee for a thorough reading of the manuscript and comments that have helped to improve the presentation of the work, particularly comments on the mass–radius relations of various models. B.M. acknowledges partial support by a project of Department of Science and Technology (DST), India, with grant No. DSTO/PPH/BMP/1946 (EMR/2017/001226).

ORCID iDs

Surajit Kalita <https://orcid.org/0000-0002-3818-6037>
 Banibrata Mukhopadhyay <https://orcid.org/0000-0002-3020-9513>

References

- Astaschenok, A. V., Capozziello, S., & Odintsov, S. D. 2013, *JCAP*, **12**, 040
 Astaschenok, A. V., Capozziello, S., & Odintsov, S. D. 2014, *PhRvD*, **89**, 103509
 Banerjee, I., Chakraborty, S., & SenGupta, S. 2020a, *PhRvD*, **101**, 041301
 Banerjee, I., Sau, S., & SenGupta, S. 2020b, *PhRvD*, **101**, 104057
 Baym, G., & Pines, D. 1971, *AnPhy*, **66**, 816
 Belyaev, V. B., Ricci, P., Šimkovic, F., et al. 2015, *NuPhA*, **937**, 17
 Berry, C. P. L., & Gair, J. R. 2011, *PhRvD*, **83**, 104022
 Bertolami, O., & Mariji, H. 2016, *PhRvD*, **93**, 104046
 Bhattacharya, M., Mukhopadhyay, B., & Mukerjee, S. 2018, *MNRAS*, **477**, 2705
 Bonazzola, S., & Gourgoulhon, E. 1996, *A&A*, **312**, 675
 Bookbinder, J. A., & Lamb, D. Q. 1987, *ApJ*, **323**, L131
 Braithwaite, J. 2009, *MNRAS*, **397**, 763
 Burrage, C., & Sakstein, J. 2018, *LRR*, **21**, 1
 Cao, Y., Johansson, J., Nugent, P. E., et al. 2016, *ApJ*, **823**, 147
 Capozziello, S., Corda, C., & de Laurentis, M. F. 2008, *PhLB*, **669**, 255
 Capozziello, S., De Laurentis, M., Farinelli, R., & Odintsov, S. D. 2016, *PhRvD*, **93**, 023501
 Casas, S., Kunz, M., Martinelli, M., & Pettorino, V. 2017, *PDU*, **18**, 73
 Chandrasekhar, S. 1931, *ApJ*, **74**, 81
 Chandrasekhar, S. 1935, *MNRAS*, **95**, 207
 Choudhuri, A. R. 2010, *Astrophysics for Physicists* (Cambridge: Cambridge Univ. Press)
 Das, U., & Mukhopadhyay, B. 2013, *PhRvL*, **110**, 071102
 Das, U., & Mukhopadhyay, B. 2014, *JCAP*, **2014**, 050
 Das, U., & Mukhopadhyay, B. 2015, *JCAP*, **5**, 045
 Dass, A., & Liberati, S. 2019, *GRGr*, **51**, 84
 De Felice, A., & Tsujikawa, S. 2010, *LRR*, **13**, 3
 Filippenko, A. V., Richmond, M. W., Branch, D., et al. 1992, *AJ*, **104**, 1543
 Ganguly, A., Gannouji, R., Goswami, R., & Ray, S. 2014, *PhRvD*, **89**, 064019
 Garmavich, P. M., Bonanos, A. Z., Krisciunas, K., et al. 2004, *ApJ*, **613**, 1120
 Glendenning, N. 2010, *Special and General Relativity: With Applications to White Dwarfs, Neutron Stars and Black Holes*, Astronomy and Astrophysics Library (New York: Springer)
 Gong, Y., & Hou, S. 2018, *Univ*, **4**, 85
 Guo, J.-Q. 2014, *IJMPD*, **23**, 1450036
 Gupta, A., Mukhopadhyay, B., & Tout, C. A. 2020, *MNRAS*, **496**, 894
 Guseinov, O. K., Novruzova, K. I., & Rustamov, I. S. 1983, *Ap&SS*, **97**, 305

- Hachisu, I., Kato, M., Saio, H., & Nomoto, K. 2012, *ApJ*, 744, 69
- Held, A., Gold, R., & Eichhorn, A. 2019, *JCAP*, 2019, 029
- Hicken, M., Garnavich, P. M., Prieto, J. L., et al. 2007, *ApJL*, 669, L17
- Hillebrandt, W., & Niemeyer, J. C. 2000, *ARA&A*, 38, 191
- Howell, D. A., Sullivan, M., Nugent, P. E., et al. 2006, *Natur*, 443, 308
- Jana, S., & Mohanty, S. 2019, *PhRvD*, 99, 044056
- Joyce, A., Lombriser, L., & Schmidt, F. 2016, *ARNPS*, 66, 95
- Kalita, S., & Mukhopadhyay, B. 2018, *JCAP*, 9, 007
- Kalita, S., & Mukhopadhyay, B. 2019a, *EPJC*, 79, 877
- Kalita, S., & Mukhopadhyay, B. 2019b, *MNRAS*, 490, 2692
- Kalita, S., & Mukhopadhyay, B. 2020, in IAU Symp. 357, White Dwarfs as Probes of Fundamental Physics: Tracers of Planetary, Stellar and Galactic Evolution, ed. M. A. Barstow (Cambridge: Cambridge Univ. Press), 79
- Kalita, S., Mukhopadhyay, B., Mondal, T., & Bulik, T. 2020, *ApJ*, 896, 69
- Kamiya, Y., Tanaka, M., Nomoto, K., et al. 2012, *ApJ*, 756, 191
- Katsuragawa, T., Nakamura, T., Ikeda, T., & Capozziello, S. 2019, *PhRvD*, 99, 124050
- Kausar, H. R., Philippoz, L., & Jetzer, P. 2016, *PhRvD*, 93, 124071
- Khokhlov, A., Mueller, E., & Hoeflich, P. 1993, *A&A*, 270, 223
- Komatsu, H., Eriguchi, Y., & Hachisu, I. 1989, *MNRAS*, 237, 355
- Landau, L., & Lifshitz, E. 1982, *Mechanics: Vol. 1* (Amsterdam: Elsevier)
- Liang, D., Gong, Y., Hou, S., & Liu, Y. 2017, *PhRvD*, 95, 104034
- Lieb, E. H., & Yau, H.-T. 1987, *ApJ*, 323, 140
- Liu, H., Zhang, X., & Wen, D. 2014, *PhRvD*, 89, 104043
- Liu, T., Zhang, X., & Zhao, W. 2018, *PhLB*, 777, 286
- Lopes de Oliveira, R., Bruch, A., Rodrigues, C. V., Oliveira, A. S., & Mukai, K. 2020, *ApJL*, 898, L40
- Maggiore, M. 2008, *Gravitational Waves: Vol. 1: Theory and Experiments* (Oxford: Oxford Univ. Press)
- Marsh, T. R., Gänsicke, B. T., Hümmelich, S., et al. 2016, *Natur*, 537, 374
- Martin, R. G., Tout, C. A., & Lesaffre, P. 2006, *MNRAS*, 373, 263
- Mazzali, P. A., Chugai, N., Turatto, M., et al. 1997, *MNRAS*, 284, 151
- Modjaz, M., Li, W., Filippenko, A. V., et al. 2001, *PASP*, 113, 308
- Moffat, J. W. 2020, arXiv:2008.04404
- Moore, C. J., Cole, R. H., & Berry, C. P. L. 2015, *CQGra*, 32, 015014
- Mott, N., & Jones, H. 1958, *The Theory of the Properties of Metals and Alloys* (New York: Dover)
- Multamäki, T., & Vilja, I. 2006, *PhRvD*, 74, 064022
- Näf, J., & Jetzer, P. 2010, *PhRvD*, 81, 104003
- Nojiri, S., Odintsov, S. D., & Oikonomou, V. K. 2017, *PhR*, 692, 1
- Nomoto, K., Iwamoto, K., & Kishimoto, N. 1997, *Sci*, 276, 1378
- Ong, Y. C. 2018, *JCAP*, 9, 015
- Otoniel, E., Franzone, B., Carvalho, G. A., et al. 2019, *ApJ*, 879, 46
- Padmanabhan, T. 2001, *Theoretical Astrophysics, Vol. 2* (Cambridge: Cambridge Univ. Press)
- Pakmor, R., Kromer, M., Röpke, F. K., et al. 2010, *Natur*, 463, 61
- Pérez, D., Romero, G. E., & Perez Bergliaffa, S. E. 2013, *A&A*, 551, A4
- Prasia, P., & Kuriakose, V. C. 2014, *IJMPD*, 23, 1450037
- Provencal, J. L., Shipman, H. L., Høg, E., & Thejll, P. 1998, *ApJ*, 494, 759
- Pun, C. S. J., Kovács, Z., & Harko, T. 2008, *PhRvD*, 78, 024043
- Ryder, L. 2009, *Introduction to General Relativity* (Cambridge: Cambridge Univ. Press)
- Saio, H., & Nomoto, K. 2004, *ApJ*, 615, 444
- Sathyaprakash, B. S., & Schutz, B. F. 2009, *LRR*, 12, 2
- Sbisà, F., Piattella, O. F., & Jorás, S. E. 2019, *PhRvD*, 99, 104046
- Scalzo, R., Aldering, G., Antilogus, P., et al. 2012, *ApJ*, 757, 12
- Scalzo, R. A., Aldering, G., Antilogus, P., et al. 2010, *ApJ*, 713, 1073
- Sedrakian, D. M., Hayrapetyan, M. V., & Sadoyan, A. A. 2005, *Ap*, 48, 53
- Shapiro, S. L., & Teukolsky, S. A. 1983, *Black holes, White Dwarfs, and Neutron Stars: The Physics of Compact Objects* (New York: Wiley)
- Sieniawska, M., & Bejger, M. 2019, *Univ*, 5, 217
- Silverman, J. M., Ganeshalingam, M., Li, W., et al. 2011, *MNRAS*, 410, 585
- Sotiriou, T. P., & Faraoni, V. 2010, *RvMP*, 82, 451
- Sousa, M. F., Coelho, J. G., & de Araujo, J. C. N. 2020, *MNRAS*, 492, 5949
- Stabile, A. 2010, *PhRvD*, 82, 064021
- Starobinsky, A. A. 1980, *PhLB*, 91, 99
- Stritzinger, M., Mazzali, P. A., Sollerman, J., & Benetti, S. 2006, *A&A*, 460, 793
- Tanaka, M., Kawabata, K. S., Yamanaka, M., et al. 2010, *ApJ*, 714, 1209
- Taubenberger, S., Benetti, S., Childress, M., et al. 2011, *MNRAS*, 412, 2735
- Taubenberger, S., Hachinger, S., Pignata, G., et al. 2008, *MNRAS*, 385, 75
- Thrane, E., & Romano, J. D. 2013, *PhRvD*, 88, 124032
- Turatto, M., Piemonte, A., Benetti, S., et al. 1998, *AJ*, 116, 2431
- Vainio, J., & Vilja, I. 2017, *GReGr*, 49, 99
- Van Den Broeck, C. 2005, *CQGra*, 22, 1825
- Will, C. M. 2014, *LRR*, 17, 4
- Yamanaka, M., Kawabata, K. S., Kinugasa, K., et al. 2009, *ApJL*, 707, L118
- Yang, L., Lee, C.-C., & Geng, C.-Q. 2011, *JCAP*, 2011, 029
- Yuan, F., Quimby, R. M., Wheeler, J. C., et al. 2010, *ApJ*, 715, 1338
- Zimmermann, M. 1980, *PhRvD*, 21, 891
- Zimmermann, M., & Szedenits, E., Jr. 1979, *PhRvD*, 20, 351